

Some attempts have been made to determine the oscillatory flow over a rippled bed as a first step towards the prediction of the sediment motion (Sleath, 1973; Sato et al., 1984; Longuet-Higgins, 1981). Numerical approaches have been used to solve momentum and continuity equations. Sleath (1973) and Sato et al. (1984) made use of finite difference schemes. Longuet-Higgins (1981) used a discrete vortex method. Even though some information on vorticity dynamics has been gained, the above methods present some drawbacks. The finite difference approaches fail when applied to conditions characterized by the relatively large values of the Reynolds number characteristic of the flow at the bottom of gravity waves. In fact a large number of grid points would be necessary in order to describe both the irrotational part of the flow and the boundary layer adjacent to the bottom; consequently an extremely large amount of CPU time would be required. The main drawback of a discrete vortex method is that it is essentially inviscid. In other words it is assumed that viscous boundary layers remain thin and passive at all times except at singular geometrical points where they separate and generate a vortex sheet. Whence if applied to the oscillatory flow over a rippled bed, a discrete vortex method fails to provide quantitative results when the boundary layer thickness is of the same order of magnitude as the ripple height and when flow separation is induced along the flat portion of the ripple profile by pressure gradients. Moreover, to the authors' knowledge no attempt has been made in the past to formulate a model able to predict sediment motion.

In the present contribution we study the oscillatory flow over a rippled bed solving the vorticity equation and Poisson equation (which relates vorticity and stream function) by means of a new numerical approach based on spectral methods and finite difference approximations. The proposed numerical approach makes it possible to obtain detailed quantitative results for values of the parameters of physical relevance using a limited amount of CPU time. Using the computed flow field we then formulate a numerical model which provides a description of the dynamics of sediment grains in suspension. The numerical results are also compared with experimental visualizations described in the first part of the present contribution.

Experimental Visualizations

In order to obtain new information on the sediment motion produced by an oscillatory flow over a rippled bed, experimental visualizations have been performed.

The experimental apparatus consists of a duct 290 cm long with a rectangular section, the width and the height of which are equal to 46 cm and 63 cm respectively. The duct is filled with water and the lower part of it is covered with sand. The fluid motion is produced by two pistons located at the ends of the duct and driven by a pneumatic motor. The amplitude and the period of the piston oscillations can be continuously varied by means of an electronic device.

Sediments in suspension are visualized using a sheet of light produced by a 2 kw lamp and an appropriate system of lenses. Sediment motion is then filmed by a standard video camera and recorded using a video tape recorder. Then a sequence of images of sediment trajectories during the flow cycle is digitalized and transferred onto the computer HP 9000. Each image is computer-analysed and different shades of grey are assigned to different light intensities. This type of procedure allows

qualitative information on sediment concentration to be gained. Moreover, looking at a sequence of images, it is also possible to obtain the trajectories of the clouds of sediments picked up and carried in suspension by the vortex structures characteristic of the flow field in the presence of ripples.

An example of the results obtained is shown in plate 1. Fluid oscillations are characterized by an amplitude S equal to 8 cm and a period T equal to 2 s. Quartz sand is used with a relative density ρ_s/ρ equal to 2.65 and a mean diameter d equal to 0.28 mm.

In photo a the flow is directed from the right to the left and the fluid velocity is maximum. The combined action of the attached boundary layer along the stoss side of the ripple and of the vortex structure generated by flow separation at the ripple crest creates a cloud of sediment just above the lee side of the ripple where a recirculating cell of fluid is located. After $T/10$ (photo b) the flow decelerates, the vortex structure strengthens and the size of recirculating cell increases. Sediments tend to be piled up at the ripple crest by the action of the vortex.

$T/10$ later (photo c) the flow goes into reverse and the vortex has almost reached its maximum strength. A lot of sediments are carried in suspension far from the bottom leaving the ripple profile at the crest. Now (photo d) the flow has reversed its direction and the main vortex structure is no longer reinforced but simply convected from the left to the right by the action of the local velocity. Sediments are carried in the same direction. Most of them tend to move close to the bottom but still a relevant part remains in suspension.

After $T/10$ (photo e) the strength of the main vortex structure decays because of viscous effects. Gravity effects tend to prevail over drag forces and sediments are slowly released along the bed profile, only few of them being in suspension. In the meantime a new vortex structure is generated by flow separation at the ripple crest and a new cloud of sediment is formed along the lee side of the ripple. Photo f, which was taken $T/2$ after photo a, shows a flow field and a sediment concentration distribution which are the mirror image of those shown in photo a. Then the sediment time development repeats similarly during the second half of the cycle.

Similar results have been obtained for different values of the parameters even though quantitative differences have been detected. In plates 2 and 3 sediment distribution is shown for T equal to 2 s, d equal to 0.28 mm and S equal to 7 cm and 10 cm respectively. It can easily be observed that in the former case less sediment is moved by the oscillatory flow and that the larger part moves close to the bottom, few sediments being picked up from the bed and carried in suspension far from the ripple profile.

The Numerical Model

Let us consider the oscillatory flow over a rippled bed and introduce a cartesian coordinate system (x^*, y^*) with the x^* -axis lying on the bottom and the y^* -axis directed upwards. Let us assume the bed profile to be described by the following equations

$$y^* = \frac{h^*}{2} \cos(k^* \xi^*) \quad x^* = \xi^* - \frac{h^*}{2} \sin(k^* \xi^*) \quad (1)$$

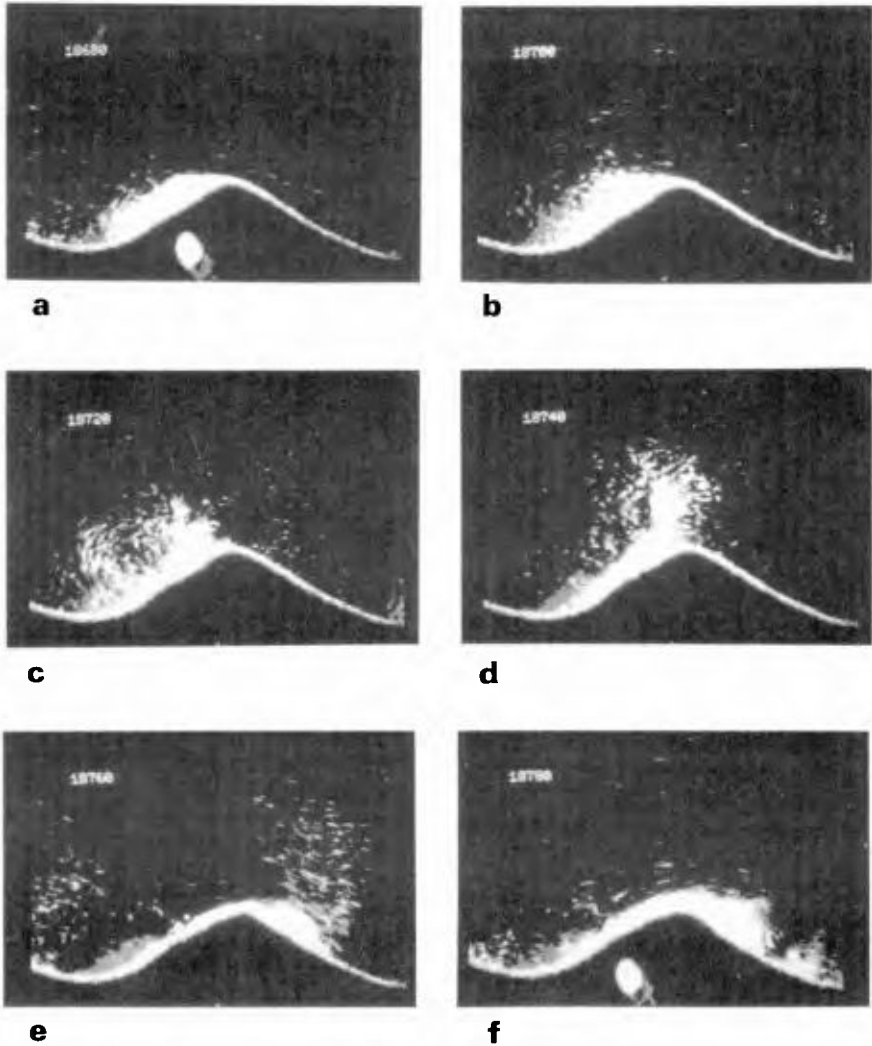


Plate 1 Experimental visualization of sediment motion over ripples in an oscillatory flow.

($S = 8$ cm, $T = 2$ s, $\rho_0/\rho = 2.65$, $d = 0.28$ mm.)

(a) $t^*/T^* = 3/4$; (b) $t^*/T^* = 17/20$; (c) $t^*/T^* = 19/20$; (d) $t^*/T^* = 21/20$;
 (e) $t^*/T^* = 23/20$; (f) $t^*/T^* = 5/4$.

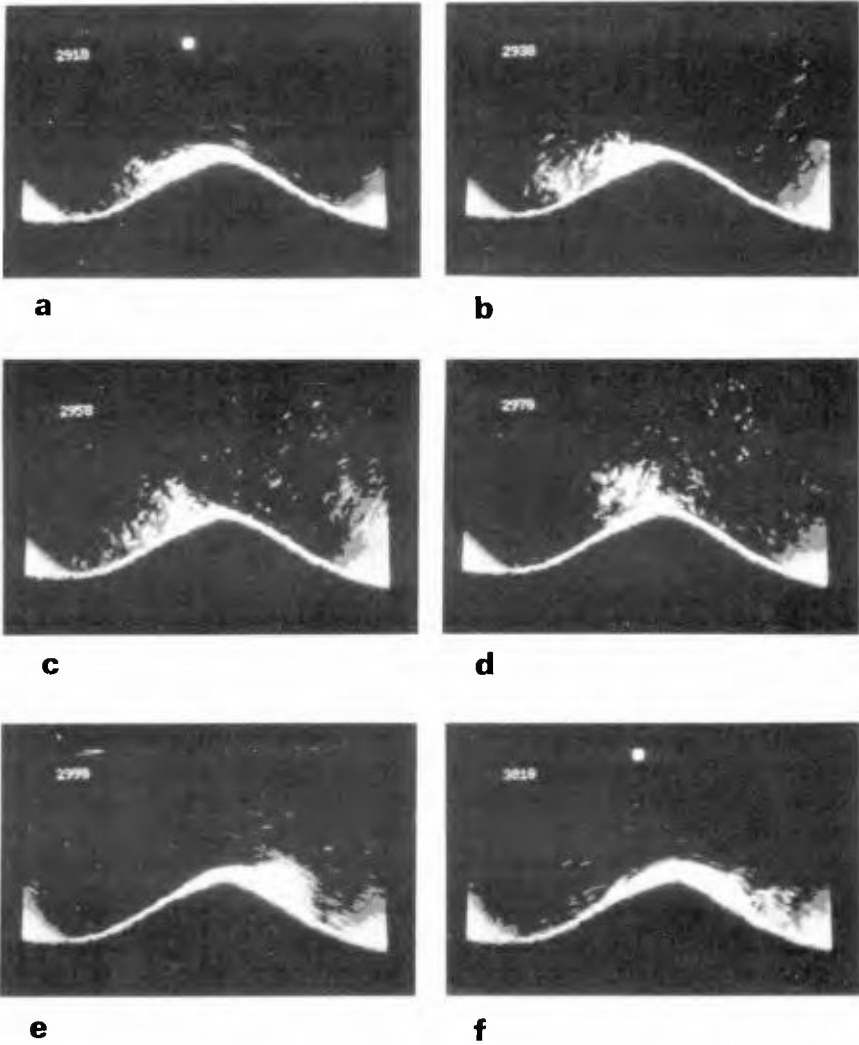


Plate 2 Experimental visualization of sediment motion over ripples in an oscillatory flow.

($S = 7$ cm, $T = 2$ s, $\rho_s/\rho = 2.65$, $d = 0.28$ mm.)

(a) $t^*/T^* = 3/4$; (b) $t^*/T^* = 17/20$; (c) $t^*/T^* = 19/20$; (d) $t^*/T^* = 21/20$;
 (e) $t^*/T^* = 23/20$; (f) $t^*/T^* = 5/4$.

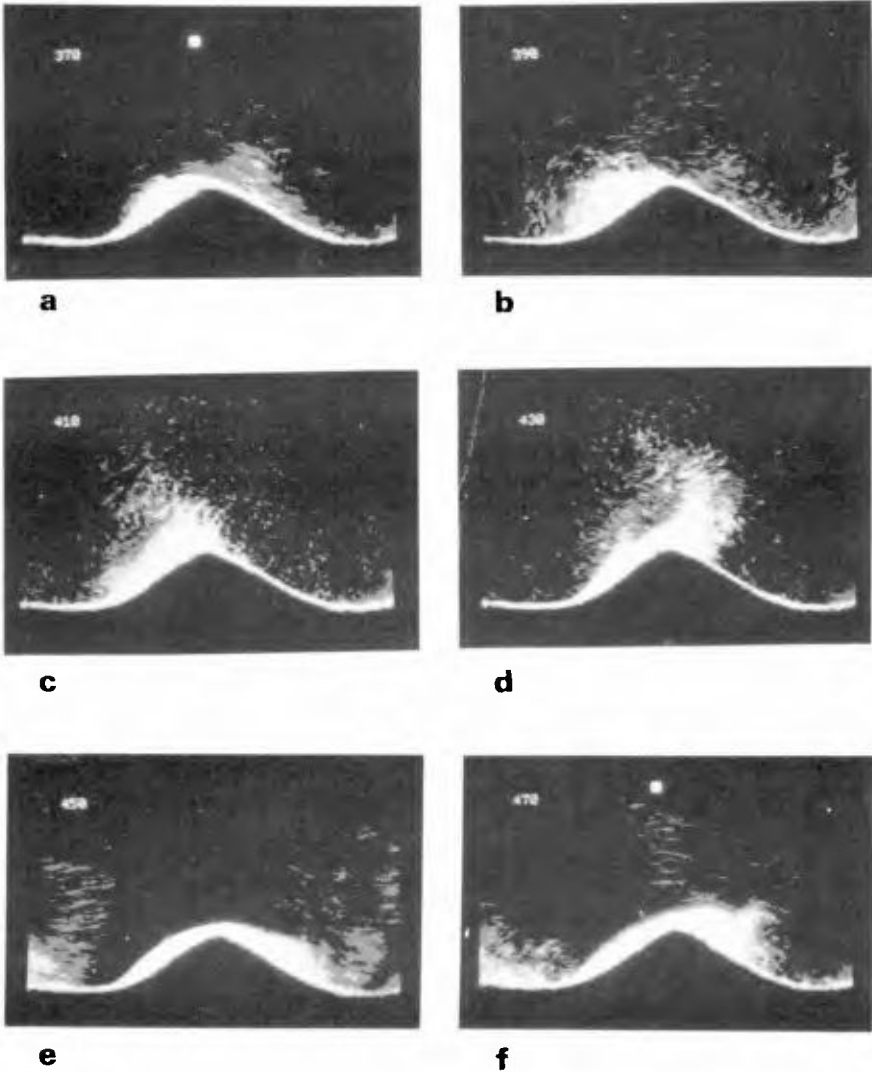


Plate 3 Experimental visualization of sediment motion over ripples in an oscillatory flow.

($S = 10$ cm, $T = 2$ s, $\rho_s/\rho = 2.65$, $d = 0.28$ mm.)

(a) $t^*/T^* = 3/4$; (b) $t^*/T^* = 17/20$; (c) $t^*/T^* = 19/20$; (d) $t^*/T^* = 21/20$;

(e) $t^*/T^* = 23/20$; (f) $t^*/T^* = 5/4$.

where $k^* = 2\pi/l^*$ is the wavenumber characteristic of the ripple, h^* , l^* its height and wavelength and ξ^* a dummy variable. As observed in real ripples the bed profile (1) exhibits crests sharper than the troughs. Moreover a comparison between experimental profiles and relationships (1) performed by Sleath (1984) shows good agreement. Assuming the flow to be two-dimensional, the differential problem governing the flow field is posed by the vorticity equation along with the Poisson equation which relates the vorticity ω^* with the stream function ψ^* and boundary conditions which force no-slip at the bottom and the matching of the flow in the bottom boundary layer with the outer irrotational flow. The latter can be assumed to be:

$$(u^*, v^*) = (U_o^* \sin 2\pi t^*/T^*, 0) \tag{2}$$

where u^* , v^* are the velocity components in the x^* and y^* directions, U_o^* and T^* the amplitude and the period of the velocity oscillations far from the bottom and t^* is time.

In order to solve the problem it is useful to introduce a new orthogonal coordinate system (ξ^*, η^*) defined by the following relationships (Sleath, 1973)

$$\xi^* = x^* + \frac{h^*}{2} e^{-k^*\eta^*} \sin(k^*\xi^*) \quad \eta^* = y^* + \frac{h^*}{2} e^{-k^*\eta^*} \cos(k^*\xi^*) \tag{3}$$

which maps the bottom profile into the line $\eta^* = 0$. Introducing the following dimensionless variables

$$t = t^* 2\pi/T^* \quad (\xi, \eta) = (\xi^*, \eta^*)/\delta^* \quad \omega = \omega^* \delta^*/U_o^* \quad \psi = \psi^*/U_o^* \delta^* \tag{4}$$

where $\delta^* = \sqrt{vT^*/\pi}$, the governing differential problem reads

$$\frac{\partial \omega}{\partial t} + \frac{R_\delta}{2J} \left[\frac{\partial \psi}{\partial \eta} \frac{\partial \omega}{\partial \xi} - \frac{\partial \psi}{\partial \xi} \frac{\partial \omega}{\partial \eta} \right] = \frac{1}{2J} \left[\frac{\partial^2 \omega}{\partial \xi^2} + \frac{\partial^2 \omega}{\partial \eta^2} \right] \tag{5}$$

$$\frac{\partial^2 \psi}{\partial \xi^2} + \frac{\partial^2 \psi}{\partial \eta^2} = -J \omega \tag{6}$$

$$\frac{\partial \psi}{\partial \xi} = \frac{\partial \psi}{\partial \eta} = 0 \quad \text{at } \eta = 0 \tag{7}$$

$$\frac{\partial \psi}{\partial \xi} \rightarrow 0 \quad \frac{\partial \psi}{\partial \eta} \rightarrow \sin t \quad \text{for } \eta \rightarrow \infty \tag{8}$$

In the equations above R_δ is the flow Reynolds number defined as $U_o^* \delta^*/\nu$ and J is the Jacobian of transformation (3). The problem is solved numerically by following a procedure which makes use of spectral methods and finite difference approximations. First of all we consider the values assumed within a ripple wavelength l by the stream function $\psi(\xi, \eta, t)$ and the vorticity $\omega(\xi, \eta, t)$ on a regular grid along the ξ -direction. Then the discrete Fourier coefficients are introduced (Orzag, 1971)

$$\psi\left(\frac{j l}{N}, \eta, t\right) = \sum_{n=0}^{N-1} \Psi_n(\eta, t) e^{i 2\pi n \frac{j}{N}}$$

$$j = 1, 2, \dots, N \quad (9)$$

$$\omega\left(\frac{j l}{N}, \eta, t\right) = \sum_{n=0}^{N-1} \Omega_n(\eta, t) e^{i 2 \pi n \frac{j}{N}}$$

Making use of (9), the problem posed by (5)–(8) is transformed into a time dependent boundary value problem in the variable η which is amenable to a classic computational approach. The solution starts with the establishment of initial conditions for the complex fields Ψ_n, Ω_n which are assumed to vanish. Then the computational cycle begins by the implementation of finite difference equations analogous to the partial differential equations for the discrete Fourier coefficients. A balance between computational costs and the attainment of accurate results made it advisable to use a first order forward scheme to approximate time derivatives and a second order central scheme to approximate spatial derivatives (Roache, 1972). It is worthwhile pointing out that a further variable $\tilde{\eta}$ was defined [$\tilde{\eta} = \ln((\eta + b)/b)$] in order to stretch the region near the bottom where the gradients of the dependent variables are larger. The value of 'b' was suitably chosen on the basis of numerical experiments. With these approximations, Ω_n inside the computational domain at a new time level is determined explicitly starting from the knowledge of Ω_n and Ψ_n at the previous time level. These updated values of Ω_n make the solution of the Poisson equation for Ψ_n possible. Indeed the implementation of a finite difference equation analogous to the Poisson equation leads to a tridiagonal system for the values assumed by Ψ_n on a regular grid along the $\tilde{\eta}$ direction. The latter system can be solved by standard methods. The last step in the computational cycle consists in calculating Ω_n on the boundary of the domain. This step is accomplished by forcing vanishing values of Ω_n far from the ripple and computing Ω_n at $\eta = 0$ according to the first order scheme suggested by Thom (1928). The above numerical procedure makes it possible to use up to 256 Fourier components and 256 grid points in the $\tilde{\eta}$ direction with a limited amount of CPU time.

Once the flow field is known, a picture of the motion of sediment grains in suspension is obtained releasing sand particles near the bottom and computing their trajectories taking into account the action of their weight, drag and lift forces. Flow acceleration effects have been ignored since the values of the Keulegan-Carpenter number characteristic of sediments are usually very large for sand at the bottom of sea waves.

It is easy to see that the equations governing the motion of a single sediment particle are

$$\begin{aligned} \frac{d\xi_p}{dt} &= \frac{v_{p\xi} R_b}{\sqrt{J} 2} & \frac{d\eta_p}{dt} &= \frac{v_{p\eta} R_b}{b e^{\eta p} \sqrt{J} 2} \\ \frac{dv_{p\xi}}{dt} &= \frac{R_b^2}{2sR_d} \left[\frac{0.5hk e^{-h\eta} \sin k\xi}{\sqrt{J} F_d^2} + \frac{3}{4} |\underline{v}_f + \underline{v}_p| (C_D(v_{f\xi} - v_{p\xi}) - C_L(v_{f\eta} - v_{p\eta})) \right] \\ \frac{dv_{p\eta}}{dt} &= \frac{R_b^2}{2sR_d} \left[\frac{1 - 0.5hk e^{-h\eta} \cos k\xi}{\sqrt{J} F_d^2} + \frac{3}{4} |\underline{v}_f - \underline{v}_p| (C_D(v_{f\eta} - v_{p\eta}) + C_L(v_{f\xi} - v_{p\xi})) \right] \end{aligned}$$

where the subscripts f and p refer to fluid and particles respectively and an underline denotes a vector.

R_d , F_d and s are the Reynolds number, the Froude number of the sediments and the ratio between sediment and fluid density respectively

$$R_d = \frac{U_o * d^*}{\nu} \quad F_d = \frac{U_o^*}{\sqrt{(s-1)gd^*}} \quad s = \frac{\rho_s}{\rho}$$

Finally it should be pointed out that the drag coefficient C_D has been computed by means of the relationship holding for the steady flow in terms of the instantaneous Reynolds number of the relative motion fluid-particle and that the ratio C_L/C_D has been assumed constant along the bottom and exponentially decaying with the distance of the particle from the ripple profile.

These approximations are likely to be very poor for large concentrations of suspended sediments; however we feel that the gross features of particle dynamics are likely to be well reproduced for low concentrations.

In figure 1 regions of clockwise and counter-clockwise vorticity are shown for $R_\delta = 100$, $k = 0.19$, $h/l = 0.15$.

The flow far from the bottom starts from rest and behaves like $\sin(t)$. It appears that clockwise vorticity is generated along the bed profile and particularly near the crest of the ripple during the first part of the cycle. By increasing t , the boundary layer thickens in the downstream side of the ripple till flow separates and vorticity of the opposite sign is generated at the bottom. Then the roll up of clockwise vorticity generates vortex structures (see figure 1_a). When the flow goes into reverse (see figure 1_b), the main vortex structure induces flow separation along the lee side of the ripple and the generation of a free shear layer characterized by vorticity of the opposite sign. In the second half of the cycle the main vortex structure is no longer reinforced but simply convected away by the local velocity.

The free shear layer originates a new vortex which couples with the previous one forming a vortex pair which travels along the bed profile moving with its self-induced velocity (see figures 1_c, 1_d). Then further counter-clockwise vorticity is shed from the ripple crest and when the flow is about to reverse its direction again, a new vortex structure is present near the crest (see figure 1_d) and the phenomenon is repeated similarly. Similar results are obtained for values of the parameters of physical relevance.

As regards the trajectories of sediment grains released near the bottom, the experimental observations are found again. Indeed looking at figure 2 where sediments in suspension are drawn for $R_\delta = 50$, $R_d = 27.5$, $F_d = 2.5$, $s = 2.65$ at different times during the cycle, it can be seen that for $t = 5.25$, when the flow is almost maximum and its direction is from right to left, a cloud of sediment is present just above the lee side of the ripple. The numerical results, in accordance with experimental findings, show that the vortex structure generated by flow separation tends to pile up sediments near the ripple crest and to carry some of them in suspension far from the ripple profile. When flow reverses, sediments are carried from left to right. Both numerical results and experimental visualizations indicate that most sediments move close to the bottom even though a relevant part is in suspension. Thus the results depicted in figure 2 show that many of the sediments rolling and sliding along the ripple profile are trapped by the new vortex forming along the lee side of the ripple. On the other hand, the sediments in suspension are

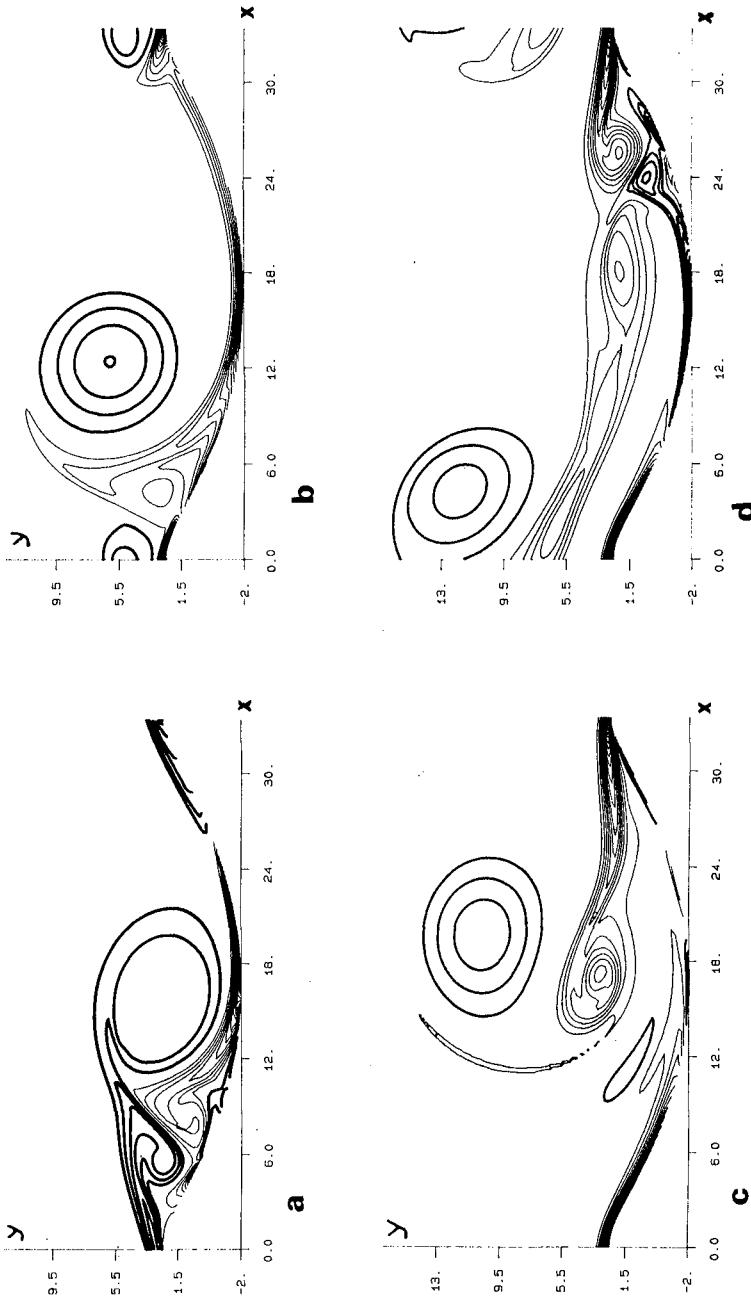


Figure 1 - Vorticity contours: $\Delta\omega = 0.15$ (— clockwise vorticity, --- counter clockwise vorticity) $R_\delta = 100$, $k = 0.19$, $h/1 = 0.15$, (a) $t = 3\pi/4$; (b) $t = \pi$; (c) $t = 5\pi/4$; (d) $t = 3\pi/2$.

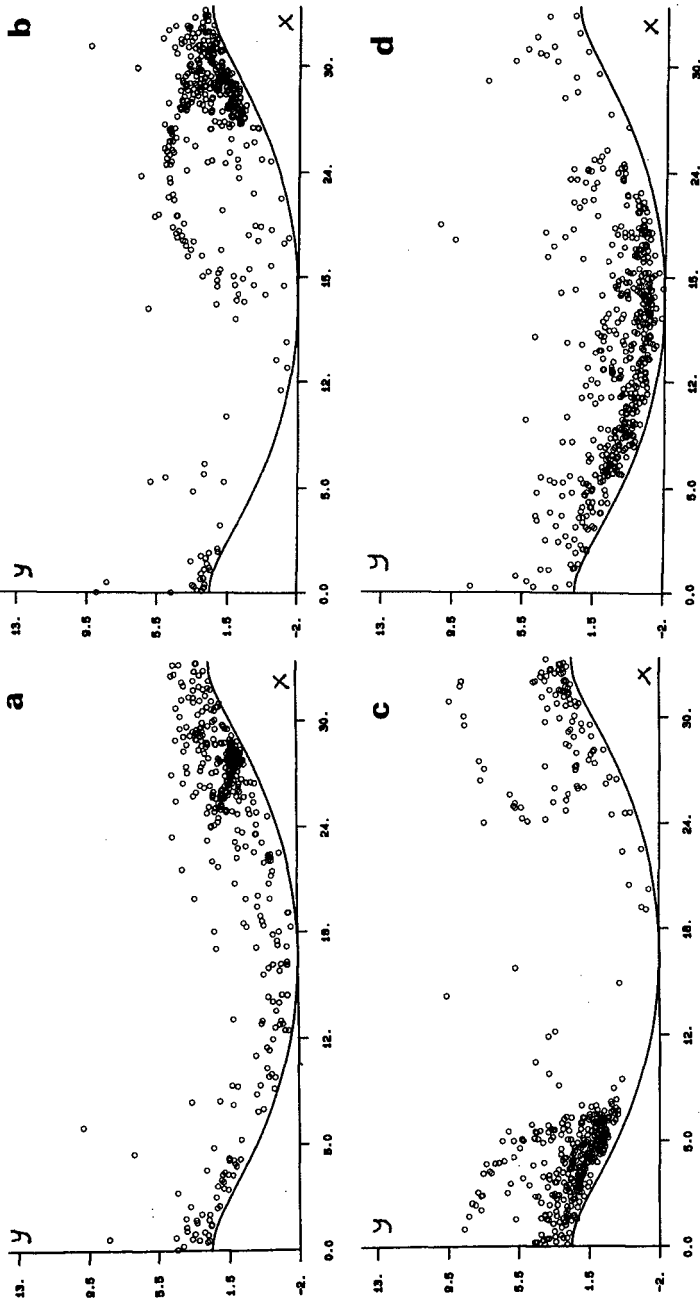


Figure 2 - Sediment particles: $R_b = 50$, $R_d = 27.5$, $F_d = 2.5$, $s = 2.65$, (a) $t = 5.25$; (b) $t = 5.95$; (c) $t = 7.0$; (d) $t = 8.05$.